J Bionic Eng 17 (2020) 303–314
DOI: https://doi.org/10.1007/s42235-020-0024-5

Journal of Bionic Engineering
http://www.springer.com/journal/42235

Synthetic Jet Control on the Propulsion Behavior of a Foil in Plunge-pitch Motion

Yadong Li[1], Guoqing Zhou[1], Jie Wu[2,3*]

1. *Liaoning General Aviation Academy*, *Shenyang Aerospace University*, *Shenyang* 110136, *China*
2. *College of Aerospace Engineering*, *Shenyang Aerospace University*, *Shenyang* 110136, *China*
3. *State Key Laboratory of Mechanics and Control of Mechanical Structures*, *Nanjing University of Aeronautics and Astronautics*, *Nanjing* 210016, *China*

Abstract

The Synthetic Jet (SJ) control on the propulsion behavior of a foil in plunge-pitch motion is examined in this work by numerical simulations. An elliptic foil with ratio of 8 performs the plunge and pitch motions synchronously. A pair of SJs with the same frequency and strength is integrated into the upper and lower surfaces of the foil. As a result, the local flow field around the foil could be obviously modified by the SJs. At the Reynolds number of 200, the effects of the inclined angle between the jet direction and the chord line, the phase angle between the SJs and the flapping motion as well as the location of SJ on the propulsion performance are systematically investigated. Compared with the pure plunging and pitching foil, it is indicated that the enhancement of mean thrust and propulsive efficiency can be obtained by the SJs with suitable working parameters. Based on the numerical analysis, it is found that the jet flow on the foil surfaces, which changes the local pressure distribution to increase the pressure difference between upper and lower surfaces, can benefit the propulsion behavior of the flapping foil.

Keywords: propulsion behavior, plunge-pitch motion, elliptic foil, synthetic jet

1 Introduction

Inspired by aquatic animals and birds/insects, flapping foils have been designed to work as propellers due to significant advantages as compared with man-made fixed-wing vehicles[1–5]. During the past several decades, the investigations on the flapping foils, *via* both experiments and numerical simulations, have been extensively conducted[6–12], and some important conclusions have been drawn. For example, the high lift generation is attributed to the intense Leading Edge Vortex (LEV) around the foil, a thrust wake is most likely an inverted Karman wake but an inverted Karman wake is not necessarily a thrust wake. In addition, some simple but efficient theories have also been proposed to quickly predict the propulsion performance[13–15]. However, due to the complex fluid-structure interactions, there still are many attempts should be made to explore the mechanisms in flapping foils.

Until now, various efforts have been made to improve the propulsion behaviors of flapping foils. Among them, the structural flexibility, including active control and passive deformation, has been frequently considered[16–19]. In the meanwhile, some attentions have also been paid to the ground effect[20–22]. On the other hand, it is known that three types of motion modes are generally used in flapping foil-based propellers, *i.e.*, pure plunge motion, pure pitch motion and combined plunge-pitch motion. But recently, other different motion trajectories have also been utilized[23–25], which include the ellipse shape and the figure-of-eight shape. In these techniques mentioned, some belong to the realm of flow control.

According to whether needing external energy or not, the flow control can be categorized into two types: passive control and active control. Compared with the passive one, the active control is more flexible and efficient. Among them, the representative is to use the Synthetic Jet Actuator (SJA)[26], which can produce zero-net-mass flux jets. Due to its simple construction

***Corresponding author:** Jie Wu
E-mail: wuj@nuaa.edu.cn

and rapid response, SJA has been widely employed for various purposes during the past decade[27]. Particularly, attributed to the quasi-two-dimensional flow profile, slot-type Synthetic Jet (SJ) is commonly used for airfoil flow control[28–31]. In these studies, the airfoil is usually stationary with a post-stall angle, and the SJ is mainly applied for the suppression of flow separation or static stall.

For the moving airfoil case, on the other hand, SJ is chosen to control the dynamic stall of a pitching airfoil. Through numerical simulations of a pitching NACA0015 airfoil, Rehman and Kontis[32] indicated that a single SJ with high frequency was suitable for lift enhancement whereas drag reduction could be achieved with large amplitude. Yen and Ahmen[33] experimentally analyzed the interaction between SJ and dynamic stall flow field. They reported that low amplitude SJ actuation would be more effective in improving the overall aerodynamic efficiency of a pitching NACA0020 airfoil compared with the high amplitude actuation. An experimental study of dynamic stall process on a finite span S809 airfoil and its control *via* SJs was conducted by Tayler and Amitay[34]. It is shown that the injection of small amount of momentum near the leading edge could completely interrupt the formation of the leading edge recirculation region. Recently, Tadjfar and Asgari[35] numerically investigated the role of excitation frequency of a tangential SJA in a pitching NACA0012 airfoil. When the excitation frequency of SJ exactly matched the pitching frequency, it was found that the performance could be far more superior to the other controlled cases in enhancing lift and reducing drag.

To the best of our knowledge, however, there is no work about the SJ control on the propulsion behaviors of flapping foils yet. Only one related work, in which a pair of SJs was applied to a plunging foil, has been done recently by Wang and Tang[36]. Since the plunging frequency was low in their study, no thrust force was generated. Due to its outstanding effectiveness for flow control, the performance of SJ applied for propulsion of a flapping foil is numerically investigated in this study. An elliptic foil with ratio of 8, which is placed in a low Reynolds number flow field, undergoes the sinusoidal plunge-pitch motion. Meanwhile, a pair of SJs with the same frequency and strength is installed on the upper and lower surfaces of the foil. The exit velocities of SJs are also sinusoidal. After fixing the flapping amplitude and frequency, the effects of the inclined angle between the jet direction and the chord line, the phase angle between the SJs and the flapping motion as well as the location of SJ on the propulsion performance are examined in detail. Based on the numerical results, the influences of SJs on the thrust force and the propulsive efficiency of the flapping foil are demonstrated.

2 Problem description and numerical method

2.1 Problem description

In this study, an elliptic airfoil with ratio of 8 is placed in a uniform flow. As sketched in Fig. 1, the foil undergoes imposed plunging and pitching motions. Same as the previous work[24,25], an imposed sinusoidal mode is used to drive the foil. So the governing equation of motions is:

$$\begin{cases} h(t) = h_m \cos(2\pi f t) \\ \theta(t) = \theta_m \sin(2\pi f t) \end{cases}, \tag{1}$$

where $h(t)$ and $\theta(t)$ are the instantaneous displacement of pitching axis and pitching angle at time t, respectively, h_m and θ_m are the corresponding amplitudes, and f is the frequency of oscillation. In this study, the pitching and plunging amplitudes are chosen as $\theta_m = 30^\circ$ and $h_m/c = 0.5$, respectively, where c is the chord length of the foil. In addition, the reduced frequency is defined as $k = 2\pi fc/U_\infty$, where U_∞ is the oncoming flow velocity. Considering the small creatures in nature, the Reynolds number based on the oncoming velocity and the chord length can be fixed at $Re = 200$.

To enhance the propulsion performance of flapping foil *via* the flow control, a pair of synthetic jets is integrated into its upper and lower surfaces. As plotted in Fig. 1, the distance from the center of SJ to the leading edge of the foil is d. In the present study, two SJs are assumed to have the same excitation frequency (f_{sj}), phase angle (ϕ) between SJ and flapping motion and jet strength (V_m), but opposite velocity directions. The excitation frequency is set to be equal to the flapping frequency, *i.e.*, $f_{sj} = f$. Moreover, the inclined angle between the jet direction and the chord line is defined as α. Thus, the time-dependent velocities of SJs can be written as:

$$V_{sj}(t) = V_m \cos(2\pi f_{sj} t + \phi), \tag{2a}$$

$$\boldsymbol{u}_{sj,\mathrm{u}} = V_{sj}\left[\cos(\theta+\alpha),\sin(\theta+\alpha)\right],\ \boldsymbol{u}_{sj,\mathrm{l}} = -\boldsymbol{u}_{sj,\mathrm{u}}, \quad (2b)$$

where $\boldsymbol{u}_{sj,\mathrm{u}}$ (or $\boldsymbol{u}_{sj,\mathrm{l}}$) is the jet velocity vector, the subscripts "u" and "l" represent the upper and lower surfaces, respectively. Additionally, the width of each SJ slot is fixed at $w = 0.1c$ in this work.

When the flapping foil works as a propeller, the mean thrust coefficient $\bar{C}_t$ and mean power coefficient $\bar{C}_p$ are two important parameters for the analysis of propulsion behavior. They are defined as:

$$\bar{C}_t = \frac{1}{T}\int_0^T C_t(t)\mathrm{d}t,\ \bar{C}_p = \frac{1}{T}\int_0^T C_p(t)\mathrm{d}t, \quad (3)$$

where C_t and C_p are the thrust coefficient and power coefficient, respectively. They are calculated by:

$$C_t = -\frac{F_\mathrm{d}}{\frac{1}{2}\rho_\infty U_\infty^2 c},\ C_p = -\frac{1}{\frac{1}{2}\rho_\infty U_\infty^3 c}\left[F_\mathrm{l}\frac{\mathrm{d}h(t)}{\mathrm{d}t} + M\frac{\mathrm{d}\theta(t)}{\mathrm{d}t}\right], \quad (4)$$

where F_d and F_l are the drag and lift forces acting on the flapping foil, M is the torque about the pitching axis, and ρ_∞ is the oncoming flow density. Thus, the propulsive efficiency can be defined as:

$$\eta_p = \bar{C}_t / \bar{C}_p. \quad (5)$$

It should be pointed out that the energy required for driving two SJs is ignored in this work.

2.2 Numerical method and validation

To simulate the viscous and incompressible flow over a plunging and pitching foil, the proposed Immersed Boundary-Lattice Boltzmann Method (IB-LBM)[37] is employed in this work. It has been well validated and widely applied for the investigations of flapping foil problems[25,38,39]. In the framework of IB-LBM, the governing equations are written as:

$$f_i(\boldsymbol{x}+\boldsymbol{e}_i\delta t, t+\delta t) = f_i(\boldsymbol{x},t) - \frac{1}{\tau}\left[f_i(\boldsymbol{x},t) - f_i^{\mathrm{eq}}(\boldsymbol{x},t)\right] + F_i\delta t, \quad (6a)$$

$$F_i = \left(1-\frac{1}{2\tau}\right)\omega_i\left(\frac{\boldsymbol{e}_i-\boldsymbol{u}}{c_s^2} + \frac{\boldsymbol{e}_i\cdot\boldsymbol{u}}{c_s^4}\boldsymbol{e}_i\right)\cdot\boldsymbol{f}, \quad (6b)$$

where $\boldsymbol{x}$ is location vector, f_i is the distribution function and f_i^{eq} is its corresponding equilibrium state, τ is the single relaxation time, e_i is the lattice velocity, δt is the time step, ω_i represent coefficients related to the lattice velocity model used, c_s is the speed of sound in lattice Boltzmann method, and $\boldsymbol{f}$ is the fluid force density that is determined by the boundary force density. By solving Eq. (6), the flow field involving the flapping foil can be achieved. More details about IB-LBM can be found in our previous work[37].

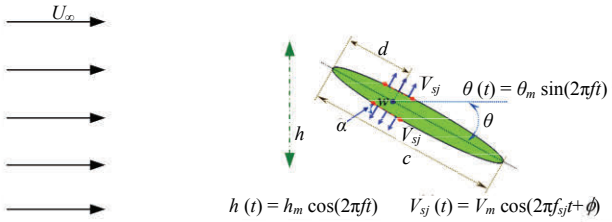

Fig. 1 Flow over a plunging and pitching foil with a pair of synthetic jets on the upper and lower surfaces.

In the following simulations, the size of computational domain is 32 c × 24 c. Initially, the flow is stationary. Free stream is imposed at the inlet and natural boundary condition is applied at the upper and lower sides and the outlet as well. A non-uniform mesh (the size is 481 c × 421 c) is used, which is fine and uniform around the foil. The mesh spacing of uniform mesh is Δ. In the current simulations, twenty flapping periods are completed for each case. It should be noted that the flow becomes periodic after the sixth flapping cycle. Same as the previous work[25], Δ = 0.00625 c is used, which is fine enough to achieve accurate results.

3 Results and discussion

Before taking the SJ effect into account, the other motion parameters of the foil used in this work should be determined firstly. It is known that the propulsion performance is sensitive to the position of pitching axis x_p from the leading edg[15]. So two pitching axis locations are checked, *i.e.*, $x_p = c/4$ and $c/2$. In order to ensure the generation of mean thrust force, the reduced frequency is chosen as $k = 2.5$. Table 1 lists the calculated mean thrust coefficient, mean power coefficient and propulsive efficiency at two different pitching axis locations. It is found that smaller x_p can result in higher propulsion performance, which is the same as the conclusion in Refs. [38, 39].

At the same time, in this work, the factors of interest related to SJs are the inclined angle between the jet

direction and the chord line (α), the phase angle between the SJs and the flapping motion (ϕ) and the distance from the center of SJ to the leading edge of the foil (d). Although the jet strength could influence the propulsion behavior, it is fixed at $V_m = U_\infty$ here. For convenience, the details of parameters used are summarized in Table 2.

3.1 Effect of jet inclined angle

To study the effect of inclined angle between the jet direction and the chord line, the phase angle and the SJ position are fixed at $\phi = 90^\circ$ and $d = c/2$, respectively. Thirteen values of α in the range of 0° – 180° are considered. Fig. 2 gives the variation of $\overline{C}_t$, $\overline{C}_p$ and η_p with respect to α. Meanwhile, the results of only a flapping foil without SJs, which are denoted as dashed lines, are also involved in the figure. From Fig. 2, it can be known that the variation trends of $\overline{C}_t$, $\overline{C}_p$ and η_p at $x_p = c/4$ and $x_p = c/2$ are identical. With the increase of α, $\overline{C}_t$ first decreases and then increases again, as shown in Fig. 2a. A minimum value appears at $\alpha = 115^\circ$ for both $x_p = c/4$ and $x_p = c/2$. As compared with the case without SJs, $\overline{C}_t$ can be improved at $0^\circ \le \alpha \le 60^\circ$ and $150^\circ \le \alpha \le 180^\circ$. A similar pattern can be found for $\overline{C}_p$ in Fig. 2b. A small difference is that $\overline{C}_p$ slightly increases before $\alpha = 30^\circ$. Moreover, it is also noted $\overline{C}_p$ is smaller than that of uncontrolled case when $\alpha \ge 60^\circ$, although the reduction is not very large. Consequently, the behavior of η_p in Fig. 2c is almost the same as that of $\overline{C}_t$. The reduction of η_p occurs at $75^\circ \le \alpha \le 120^\circ$, whilst the maximum improvement of η_p appears at $\alpha = 30^\circ$.

Besides the propulsion performance, the flow patterns are affected when the synthetic jets are used. Fig. 3 presents the vorticity contours of cases with and without SJs at $x_p = c/2$ in the first half flapping period. The parameters of SJ are $\phi = 90^\circ$, $d = c/2$, $\alpha = 0^\circ$ and 90°. It is noted the contours for three different cases have the same values in each sub-figure.

From Eq. (1), it is known that the foil has left its highest position of plunging motion at $t/T = 1/8$. For the uncontrolled case (Fig. 3a), two recirculation regions along the upper and lower surfaces are formed around the leading edge of the foil. For the case with SJs at $\alpha = 0^\circ$ (Fig. 3b), the tangential jets clearly destroy two

Table 1 Propulsion performance without SJs

x_p	$\overline{C}_t$	$\overline{C}_p$	η_p (%)
$c/4$	0.262	2.002	13.10
$c/2$	0.179	1.559	11.47

Table 2 All parameters of SJ examined in this work

Inclined angle (α)	Phase angle (ϕ)	SJ position (d)
0° – 180°	0° – 330°	$c/4$ – $3c/4$

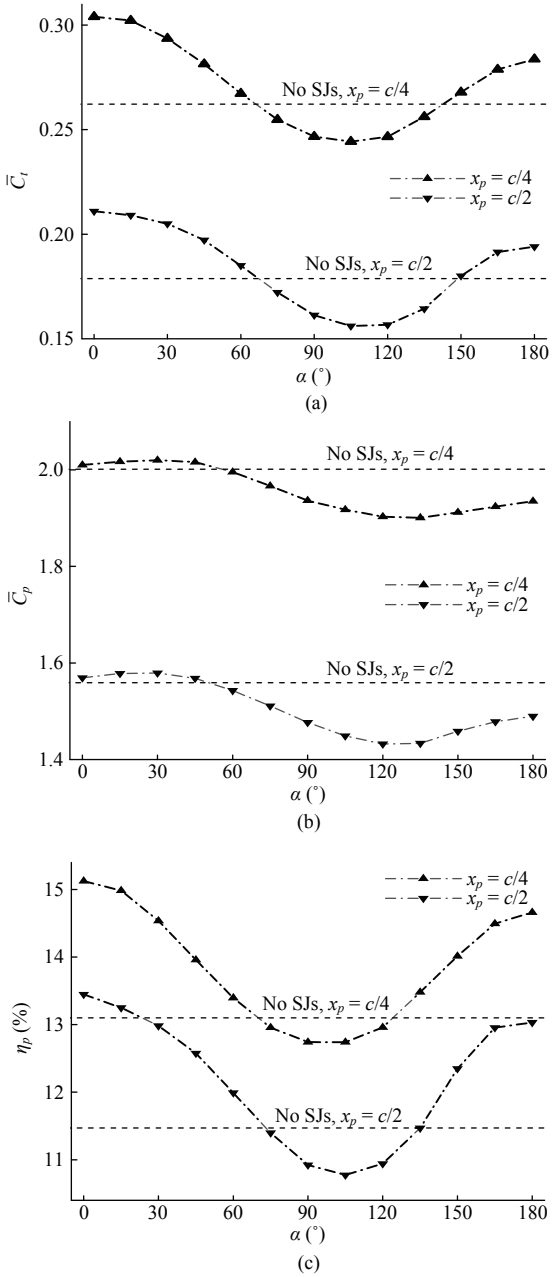

Fig. 2 Comparison of (a) mean thrust coefficient, (b) mean power coefficient and (c) propulsive efficiency for flow over a plunging and pitching foil with SJs at $\phi = 90^\circ$ and $d = c/2$.

recirculation regions. But for the case of $\alpha = 90^{\circ}$, the recirculation regions are weakly hampered by the vertical jets (Fig. 3c). When the foil comes to the medium position of plunging motion at $t/T = 1/4$, the recirculation regions are enlarged. Meanwhile, the effect of SJs is also strengthened. As the foil further moves downwards, the phenomenon of vortex shedding happens. Since the strength of SJs is weakened, the vorticity around the foil is also less influenced.

Based on the results above, it is noticed that the jet inclined angle can clearly modify the performance of the flapping foil with SJs. During a specific range of inclined angle, the mean thrust coefficient and propulsive efficiency can be enhanced as compared with the uncontrolled case.

3.2 Effect of jet phase angle

To check the effect of phase angle between the SJs and the flapping motion, twelve values of ϕ are chosen from 0° to 330° with the interval of 30°. Again, the SJ position is fixed at $d = c/2$. Two typical inclined angles are selected, *i.e.*, $\alpha = 0^{\circ}$ and $\alpha = 90^{\circ}$, which respectively corresponds to propulsion enhancement and reduction. Fig. 4 illustrates $\overline{C}_t$, $\overline{C}_p$ and η_p varying with ϕ. Again, the results without SJs are involved in the figure. Same as Fig. 2, the behaviors of $\overline{C}_t$, $\overline{C}_p$ and η_p at two pitching axis positions are very close to each other for both $\alpha = 0^{\circ}$ and $\alpha = 90^{\circ}$. As can be seen from Fig. 4a, $\overline{C}_t$ first increases and then decreases with ϕ for the case of $\alpha = 0^{\circ}$. Moreover, $\overline{C}_t$ is always larger than that of uncontrolled

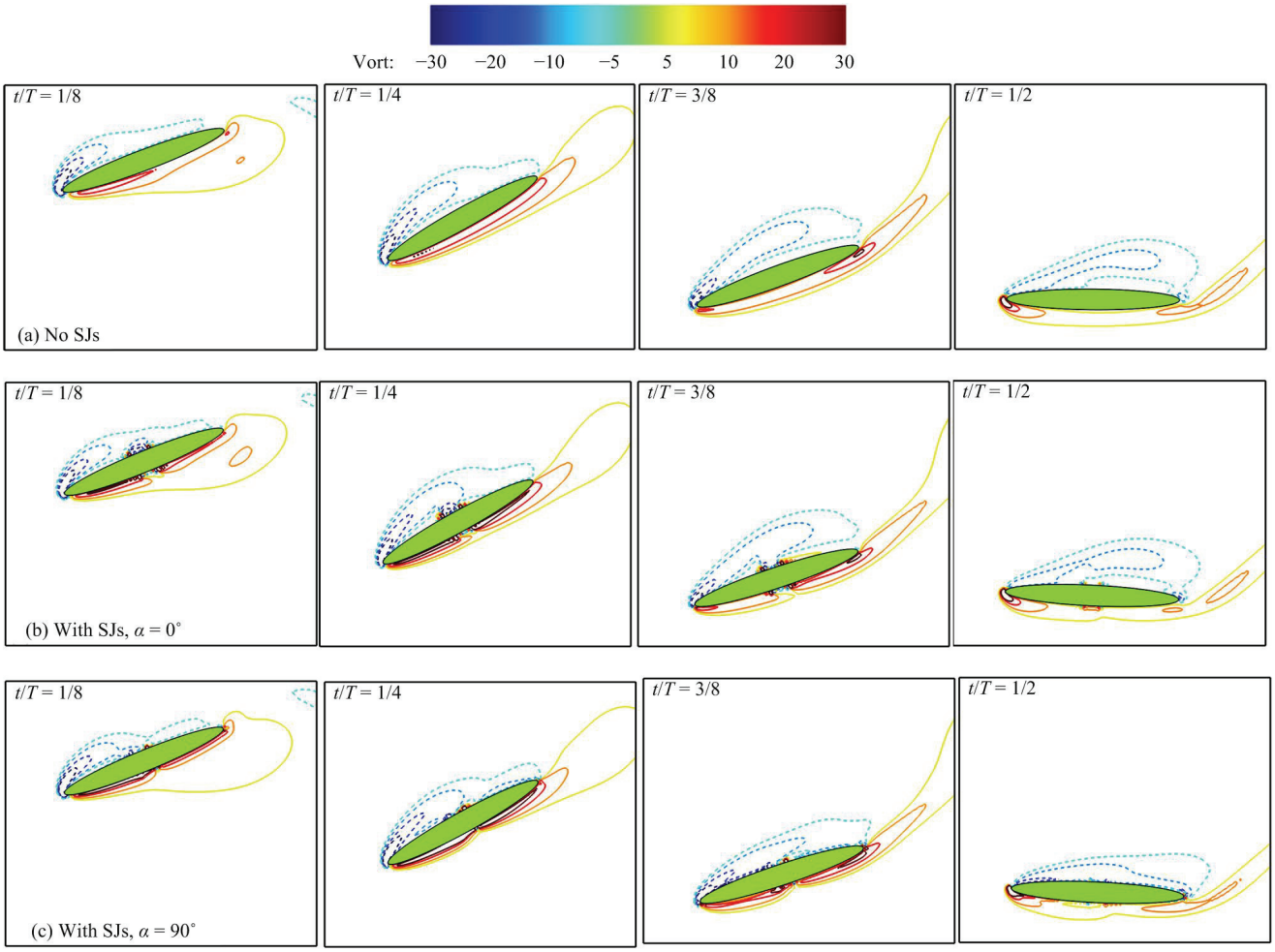

Fig. 3 Vorticity contours in the first half flapping period at $x_p = c/2$. (a) No SJs; (b) with SJs at $\alpha = 0^{\circ}$; (c) with SJs at $\alpha = 90^{\circ}$. Other parameters of SJ are $\phi = 90^{\circ}$ and $d = c/2$.

case. While for the case of α = 90°, the variation of $\bar{C}_t$ with respect to ϕ is a little more complex, which is always smaller than the case without SJs. Thus, it seems that ϕ cannot greatly modify $\bar{C}_t$. From Fig. 4b, however, some reduction of $\bar{C}_p$ can be found for α = 0°, whilst there is no clear change of $\bar{C}_p$ for α = 90°. So the same as $\bar{C}_t$, $\bar{C}_p$ is also not sensitive to ϕ. As a result, the variation trend of η_p, as shown in Fig. 4c, is nearly the same as that of $\bar{C}_t$. In particular, the maximum values of η_p for $x_p = c/4$ and $x_p = c/2$ appear at ϕ = 150° and ϕ = 90°, respectively.

Similar to the inclined angle effect, the flow patterns are also influenced by using different jet phase angle. Fig. 5 provides the pressure coefficient contours of cases with and without SJs at $x_p = c/4$ in the first half flapping period. The parameters of SJ are α = 0°, $d = c/2$, ϕ = 0° and 90°. Again, the contours for three different cases have the same values in each sub-figure. At t/T = 1/8 (Fig. 5a), a wide negative pressure region covers the upper surface of the foil, while a small positive pressure region is located around the leading edge of lower surface. When the SJs are used, the pressure fields around the jet slots are changed more or less. At t/T = 1/4 (Fig. 5b), the sizes of both negative and positive pressure regions are increased. For the cases with SJs, the negative pressure region on the foil upper surface is further spread, but the positive pressure region is shrunk slightly. In addition, a very small positive pressure region is formed around the jet slot of lower surface for ϕ = 90°. At t/T = 3/8, the positive pressure region has occupied about half part of lower surface, while no clear change of negative pressure region happens. When the SJs work, this positive pressure region is broken, and the small positive pressure region grows up. At t/T = 1/2, there is no obvious positive pressure region around the foil, and the use of SJs only changes the local pressure field to some extent.

Based on the above results, it is shown that the jet phase angle also influences the behavior of the flapping foil with SJs. The mean thrust coefficient is increased at some phase angles, while the mean power coefficient is decreased at other phase angles. The possible reason is that the pressure field along the foil surface is redistributed by the SJs.

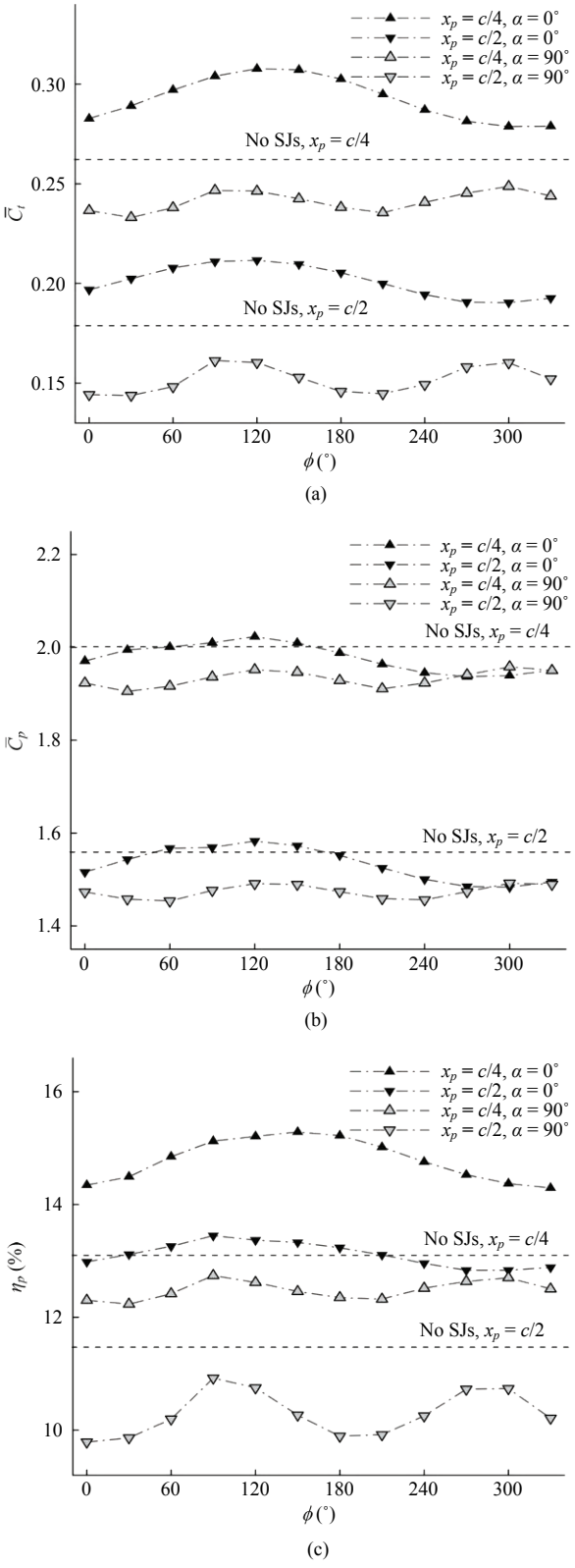

Fig. 4 Comparison of (a) mean thrust coefficient, (b) mean power coefficient and (c) propulsive efficiency for flow over a plunging and pitching foil with SJs at $d = c/2$.

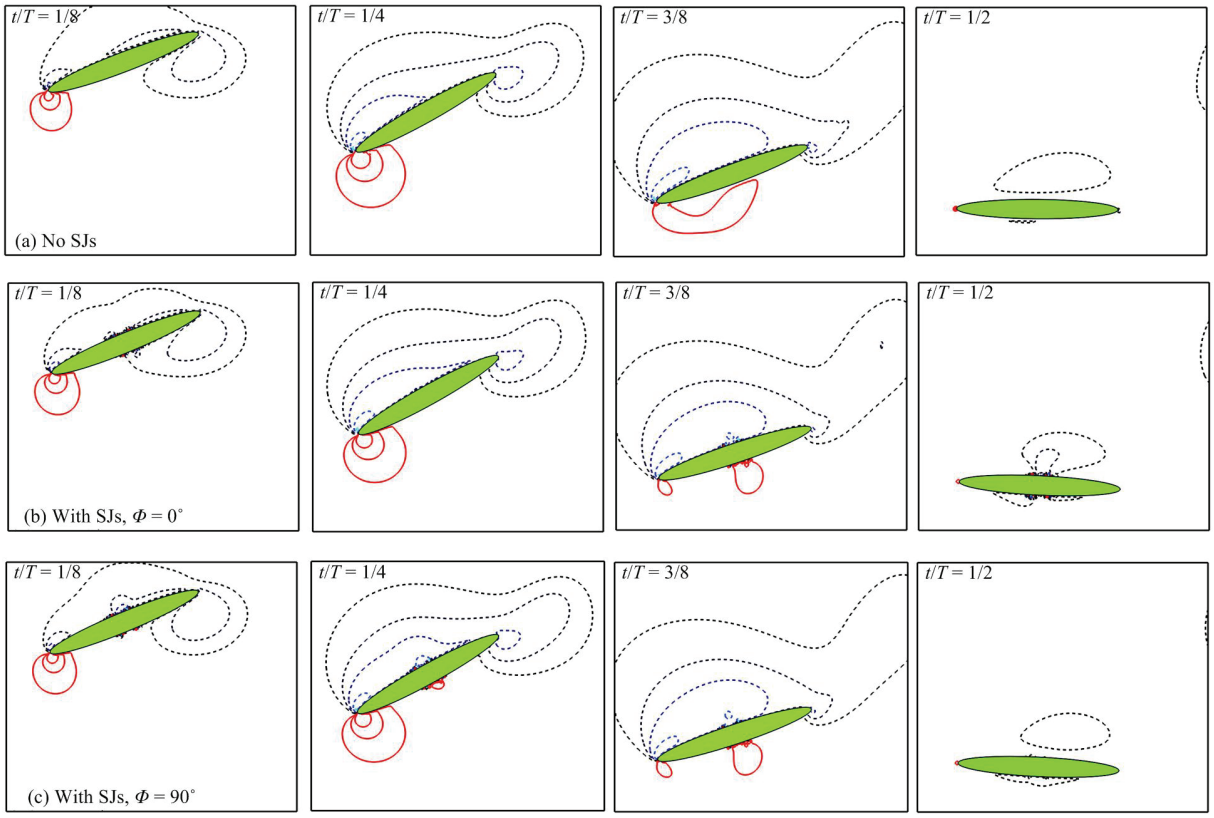

Fig. 5 Pressure coefficient contours in the first half flapping period at $x_p = c/4$. (a) No SJs; (b) with SJs at $\phi = 0^\circ$; (c) with SJs at $\phi = 90^\circ$. Other parameters of SJ are $\alpha = 0^\circ$ and $d = c/2$.

3.3 Effect of SJ position

Besides the inclined angle and the phase angle, the location where the SJs work plays an important role in the propulsion performance. To check this effect, the phase angle is fixed at $\phi = 90^\circ$. In addition, $\alpha = 0^\circ$ and $\alpha = 90^\circ$ are still selected. Five SJ positions are considered, *i.e.*, $d = c/4$, $c/3$, $c/2$, $2c/3$ and $3c/4$. Similar to Figs. 2 and 4, $\overline{C}_t$, $\overline{C}_p$ and η_p changing with d are plotted in Fig. 6. The results without SJs are still involved in the figure. From Fig. 6a, it can be found that the variation trend of $\overline{C}_t$ at $\alpha = 0^\circ$ is significantly different from that at $\alpha = 90^\circ$. Specifically, $\overline{C}_t$ at $\alpha = 0^\circ$ can monotonically increase with d, but it decreases with d monotonically at $\alpha = 0^\circ$. For a given x_p, therefore, $\overline{C}_t$ at $\alpha = 90^\circ$ is larger than that at $\alpha = 0^\circ$ when $d \le c/3$, and the situation reverses when $d \ge c/2$. From Fig. 6b, on the other hand, it is known that the change of $\overline{C}_p$ with d is relatively small. Concretely, $\overline{C}_p$ at $\alpha = 0^\circ$ just shows slight modification and no reduction is observed as compared with the case without SJs. But $\overline{C}_p$ at $\alpha = 90^\circ$ can increase with d smoothly and it is smaller than that of no SJs when $d \le c/2$. Taken together, a high η_p can be produced for the case of $\alpha = 90^\circ$ when $d \le c/3$, which is even larger than that of $\alpha = 0^\circ$ at $d = 3c/4$. The maximum values of η_p here are 18.76% and 18.10% for $x_p = c/4$ and $c/2$, respectively (The corresponding enhancement of η_p can reach 43.21% and 57.81%, respectively). Based on the results shown in Fig. 6, it is indicated that the propulsion behavior is greatly dependent to the SJ position.

3.4 Mechanism of propulsion modification

To dig into the mechanism of propulsion modification due to the synthetic jet control, the behaviors of thrust force, lift force and torque should be analyzed in detail. To this end, the cases at $\alpha = 90^\circ$ and $\phi = 90^\circ$ considered. Two sets of SJ positions together with pitching axis locations are selected, *i.e.*, $d = c/4$ with $x_p = c/4$ that corresponds to the efficiency improvement situation and $d = 3c/4$ with $x_p = c/2$ that corresponds to the efficiency reduction status. As a reference, the cases without SJs at $x_p = c/4$ and $c/2$ are also taken into account.

From Eq. (4), it is known that the power coefficient has two components. One is caused by plunge C_{ph}, which is determined by the lift coefficient C_l and the heaving velocity $(\mathrm{d}h/\mathrm{d}t)/U_\infty$. The other is due to pitch $C_{p\theta}$, which is determined by the torque coefficient C_m and the pitching velocity $(\mathrm{d}\theta/\mathrm{d}t)c/U_\infty$. Fig. 7 then provides the time evolution of C_t, $-C_l$, $(\mathrm{d}h/\mathrm{d}t)/U_\infty$, C_{ph}, $-C_m$, $(\mathrm{d}\theta/\mathrm{d}t)c/U_\infty$ and $C_{p\theta}$ over a flapping period.

As can be seen from Fig. 7a, for the case of $d = c/4$ with $x_p = c/4$, the use of SJs clearly increases C_t in the time range of $0 \le t/T \le 0.2$ and $0.6 \le t/T \le 0.8$. In contrast, C_t is obviously decreased in the time range of $0 \le t/T \le 0.3$ and $0.7 \le t/T \le 1$ for the case of $d = 3c/4$ with $x_p = c/2$. This might explain the enhancement or reduction of $\overline{C}_t$ as compared with the uncontrolled case.

On the other hand, it can be observed from Fig. 7b that C_l and $(\mathrm{d}h/\mathrm{d}t)/U_\infty$ have a good synchronization when the pitching axis is located at $x_p = c/4$. As a result, C_{ph} has two peaks with large values, as shown in Fig. 7c. Moreover, the SJs decrease the magnitude of C_l nearly during the second half flapping period. When the pitching axis is shifted to $x_p = c/2$, however, the synchronization between C_l and $(\mathrm{d}h/\mathrm{d}t)/U_\infty$ is down. Then the peak values of C_{ph} drop greatly. In addition, it is noted that the magnitude of C_l can be increased by the SJs more or less in the time range of $0.6 \le t/T \le 0.9$. Consequently, both the reduction and enhancement of $\overline{C}_{p_h}$ can be found in Fig. 7c.

As shown in Fig. 7d, the synchronization between C_m and $(\mathrm{d}\theta/\mathrm{d}t)c/U_\infty$ is not so good. For the case of $x_p = c/4$, the phase difference between C_m and $(\mathrm{d}\theta/\mathrm{d}t)c/U_\infty$ is about $\pi/2$. So $C_{p\theta}$ vibrates around a zero value line, as plotted in Fig. 7e. Similar to C_l, C_m is also changed by the SJs. Its magnitude is smoothly increased during some parts of period. For the case of $x_p = c/2$, on the other hand, the phase difference between C_m and $(\mathrm{d}\theta/\mathrm{d}t)c/U_\infty$ is about $\pi/4$. Then $C_{p\theta}$ can change around a positive value line. When the SJs are used, the magnitude of C_m is decreased mainly during the first half period. Therefore, as presented in Fig. 7e, the magnitude of $\overline{C}_{p_\theta}$ is enhanced at $d = c/4$ with $x_p = c/4$ and reduced at $d = 3c/4$ with $x_p = c/2$. Nevertheless, the magnitude of $\overline{C}_{p_\theta}$ is small, and then its contribution to $\overline{C}_p$ is not obvious, even when the synthetic jet control is em ployed.

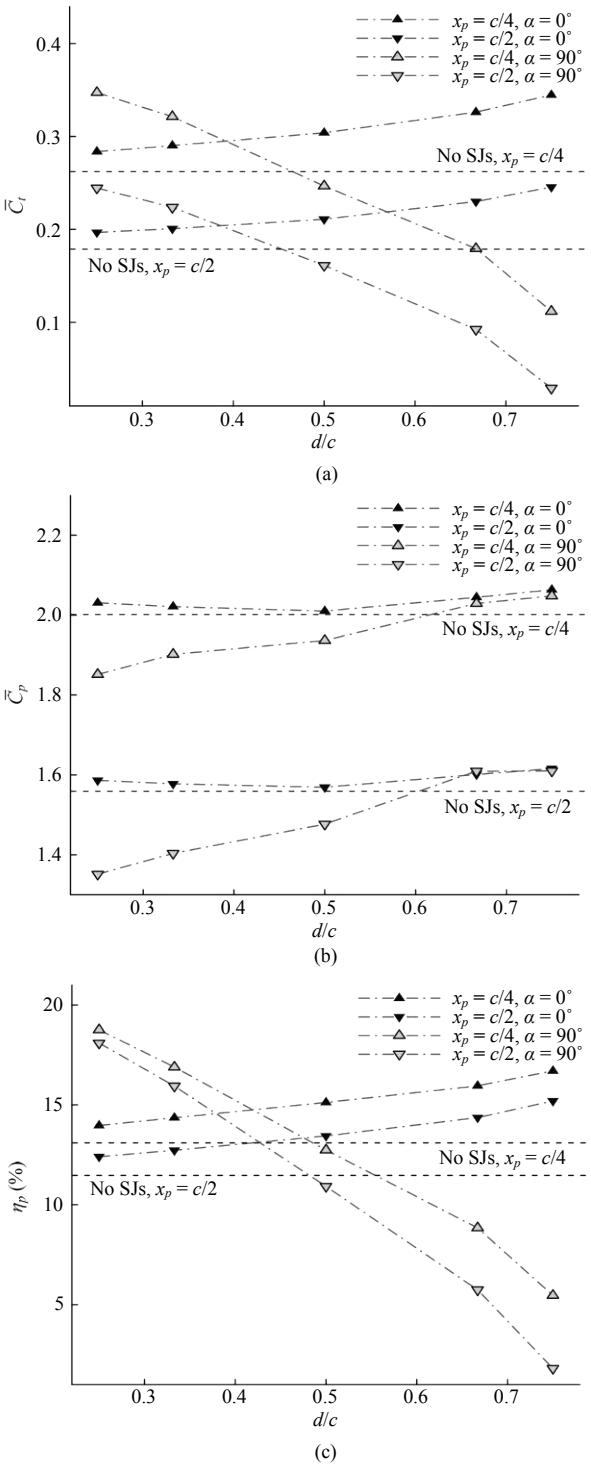

Fig. 6 Comparison of (a) mean thrust coefficient, (b) mean power coefficient and (c) propulsive efficiency for flow over a plunging and pitching foil with SJs at $\phi = 90°$.

To further investigate the changes of C_t and C_l (since $\overline{C}_{p_\theta}$ only slightly modifies $\overline{C}_p$, C_m is not further considered), the flow field near the flapping foil could be

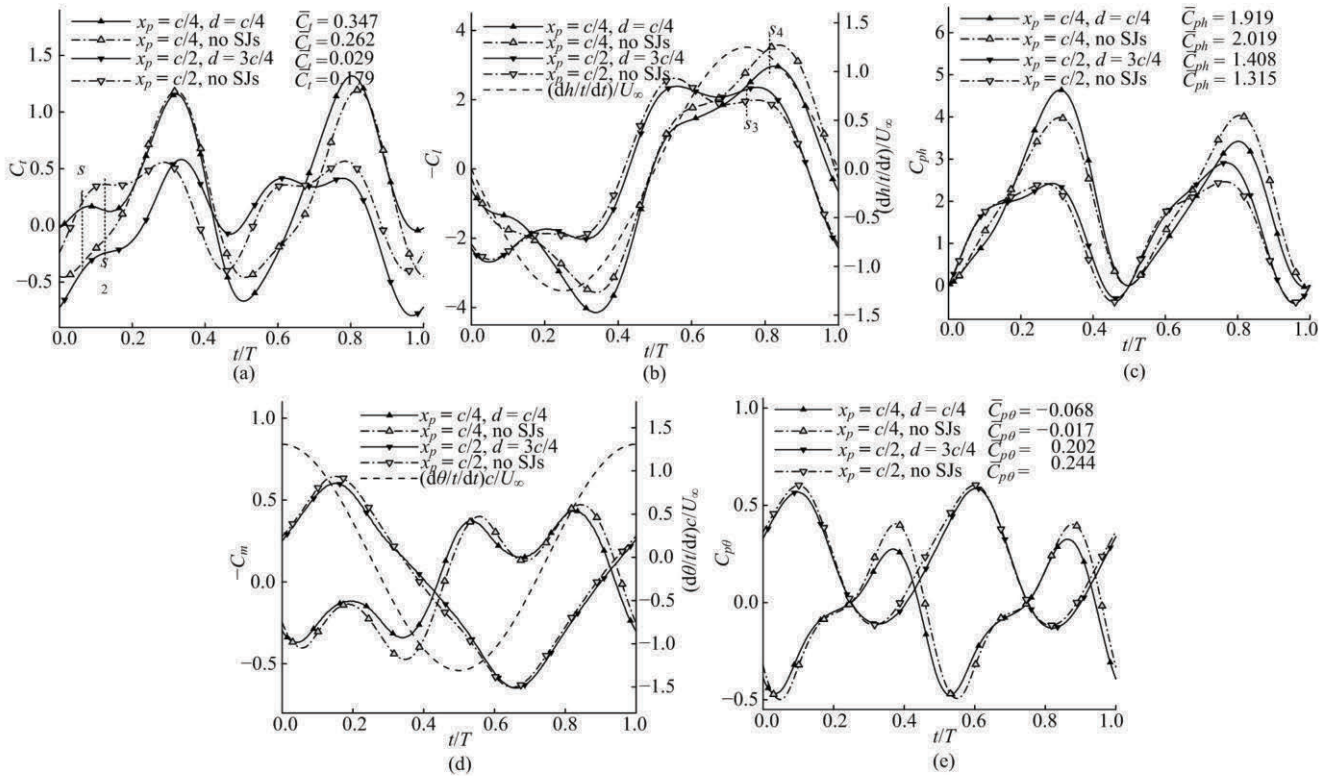

Fig. 7 Time evolution of (a) thrust coefficient, (b) lift coefficient, plunging velocity, (c) power coefficient due to plunge, (d) torque coefficient, pitching velocity and (e) power coefficient due to pitch over a flapping period for flow over a plunging and pitching foil with and without SJs.

checked. Figs. 8 and 9 illustrate the pressure coefficient contours at four different instants (denoted as s_1–s_4 in Figs. 7a and 7b), respectively. The contour range is the same as that in Fig. 5.

At the instant of $t/T = 1/16$ (*i.e.* s_1 in Fig. 7a), the foil just left its highest position of plunging motion. Simultaneously, it is rotating in the clockwise direction with a small angle of attack. For the uncontrolled case of $x_p = c/4$, as shown in Fig. 8a, a negative pressure region covers the whole upper surface of the foil, and another negative pressure region is also below the lower surface of back half of the foil. Meanwhile, a small positive pressure region is attached to the leading edge. Therefore, the pressure difference of the foil along the horizontal direction generates a drag force (*i.e.*, negative thrust force, as can be seen in Fig. 7a). When the SJs are placed at $d = c/4$, the negative pressure around the leading edge of upper surface is strengthened. At the same time, the positive pressure region is significantly shrunk. As a result, the pressure difference along the horizontal direction is changed, and a thrust force with small value appears.

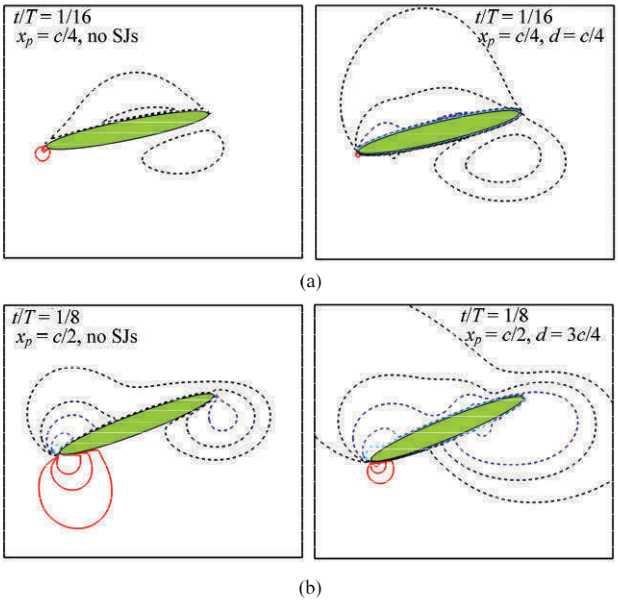

Fig. 8 Pressure coefficient contours at two instants in the first half period. (a) s_1: $t/T = 1/16$; (b) s_2: $t/T = 1/8$.

At the moment of $t/T = 1/8$ (*i.e.* s_2 in Fig. 7a), the foil keeps moving downwards with the increased angle of attack. For the case of no SJs and $x_p = c/2$, as shown

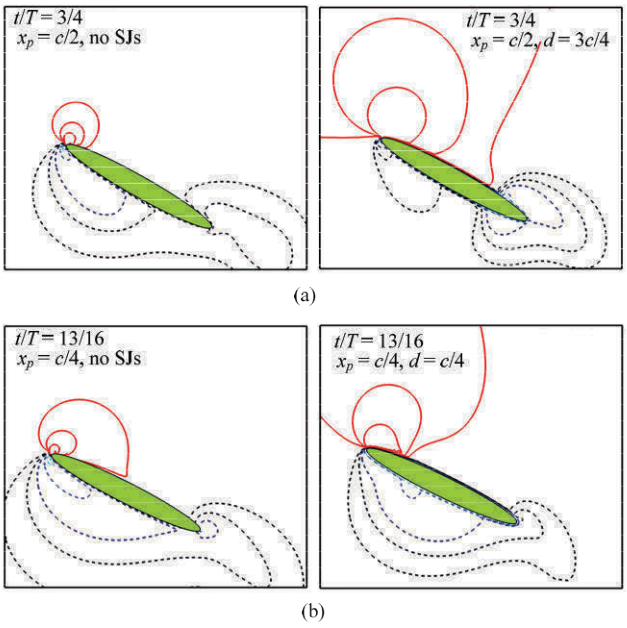

Fig. 9 Pressure coefficient contours at two instants in the second half period. (a) s_3: $t/T = 3/4$; (b) s_4: $t/T = 13/16$.

in Fig. 8b, the positive pressure region around the leading edge is greatly enlarged as compared with situation at $t/T = 1/16$, and it also partially occupies the lower surface. Thus, a pressure component along the horizontal direction points upstream. Although there is a negative pressure region around the trailing edge of lower surface, the pressure difference of the foil along the horizontal direction still can produce a thrust force (Fig. 7a). When the SJs are installed at $d = 3c/4$, the positive pressure region is obviously shrunk and the negative pressure on the upper surface is strengthened. This greatly reduces the horizontal pressure component or even makes it point downstream. Moreover, the negative pressure region on the lower surface is expanded clearly. Therefore, the pressure difference of the foil along the horizontal direction results in a drag force.

At $t/T = 3/4$ (s_3 in Fig. 7b), the foil has finished its downstroke and just reaches the middle position of upstroke. As plotted in Fig. 9a, the pressure distribution for the uncontrolled case of $x_p = c/2$ is nearly opposite to that at $t/T = 1/8$. So there exists a negative lift force (Fig. 7b). For the controlled case of $d = 3c/4$, the positive pressure region on the upper surface is stretched greatly. Thus, the pressure difference along the vertical direction of the foil is increased, which then enhances the magnitude of lift force.

At $t/T = 13/16$ (s_4 in Fig. 7b), the foil keeps moving upwards. For the case without SJs at $x_p = c/4$, as given in Fig. 9b, the positive pressure region around the leading edge is expanded as compared with status at $t/T = 3/4$. Meanwhile, the negative pressure on the lower surface is reinforced. Then a higher negative lift force is generated (Fig. 7b). For the case with SJs at $d = c/4$, the positive pressure region on the upper surface is contracted to some extent, whilst there is no clear change of negative pressure region on the lower surface. As a consequence, the magnitude of lift force is reduced.

Based on the results in Figs. 7–9, it is known that the suitable increase in thrust force and decrease in lift force, which is caused by the modification of pressure distribution along the foil surface, are the key issue for the enhancement of propulsion behavior with the use of synthetic jet.

4 Conclusion

In this study, a pair of synthetic jets is utilized to improve the propulsion performance of an oscillating foil in a low Reynolds number flow. An elliptic foil with ratio of 8 executes the plunge and pitch motions. The SJs have the same frequency and strength, which are placed on the upper and lower surfaces of the foil. At the fixed Reynolds number (200), the parametric studies about the inclined angle between the jet direction and the chord line, the phase angle between the SJs and the flapping motion as well as the location of SJ are carried out *via* numerical simulations.

Based on the results obtained, it is demonstrated that the use of SJs can affect both the force behavior and propulsive efficiency. Compared with the flapping foil without SJs, the propulsive efficiency can be improved under the condition of appropriate SJ parameters. Particularly, η_p of foil operating at $x_p = c/4$ with $k = 2.5$ can be enhanced from 13.1% to 18.76% at $\alpha = 90^\circ$, $\phi = 90^\circ$ and $d = c/4$. According to the numerical analysis, it is shown that the efficiency enhancement due to the use of SJs mainly benefits from the increased thrust force and decreased lift force. The potential mechanism is that the pressure on the surface of the foil is redistributed attributed to the proper flow control of synthetic jet. On the other hand, it should be pointed out that other SJ parameters such as the jet strength also may modify the

propulsion performance of the plunge-pitch foil. In the future work, more parametric analyses will be done.

Acknowledgment

The authors acknowledge the support of the National Natural Science Foundation of China (Grant No. 11622219) and the Natural Science Foundation of Jiangsu Province (Grant No. BK20191271). This work is also supported by the Priority Academic Program Development of Jiangsu Higher Education Institutions (PAPD).

References

[1] Lighthill M J. Hydromechanics of aquatic animal propulsion. *Annual Review of Fluid Mechanics*, 1969, **1**, 413–449.

[2] Maxworthy T. The fluid dynamics of insect flight. *Annual Review of Fluid Mechanics*, 1981, **13**, 329–350.

[3] Wang Z J. Dissecting insect flight. *Annual Review of Fluid Mechanics*, 2005, **37**, 183–210.

[4] Platzer M F, Jones K D, Young J, Lai J C S. Flapping wing aerodynamics: Progress and challenges. *AIAA Journal*, 2008, **46**, 2136–2149.

[5] Wu T Y. Fish swimming and bird/insect flight. *Annual Review of Fluid Mechanics*, 2011, **43**, 25–58.

[6] Ellington C P, van den Berg C, Willmott A P, Thomas A L R. Leading-edge vortices in insect flight. *Nature*, 1996, **384**, 626–630.

[7] Anderson J M, Streitlien K, Barret K S, Triantafyllou M S. Oscillating foils of high propulsive efficiency. *Journal of Fluid Mechanics*, 1998, **360**, 41–72.

[8] Dickinson M H, Lehmann F O, Sane S P. Wing rotation and the aerodynamic basis of insect flight. *Science*, 1999, **284**, 1954–1960.

[9] Sun M, Tang J. Unsteady aerodynamic force generation by a model fruit fly wing in flapping motion. *Journal of Experimental Biology*, 2002, **205**, 55–70.

[10] Lehmann F O, Pick S. The aerodynamic benefit of wing-wing interaction depends on stroke trajectory in flapping insect wings. *Journal of Experimental Biology*, 2007, **210**, 1362–1377.

[11] Baik Y S, Bernal L P, Granlund K, Ol M V. Unsteady force generation and vortex dynamics of pitching and plunging aerofoils. *Journal of Fluid Mechanics*, 2012, **709**, 37–68.

[12] Au L T K, Phan V H, Park H C. Longitudinal flight dynamic analysis on vertical takeoff of a tailless flapping-wing micro air vehicle. *Journal of Bionic Engineering*, 2018, **15**, 283–297.

[13] Das A, Shukla R K, Govardhan R N. Existence of a sharp transition in the peak propulsive efficiency of a low-*Re* pitching foil. *Journal of Fluid Mechanics*, 2016, **800**, 307–326.

[14] Fernandez-Feria R. Linearized propulsion theory of flapping airfoils revisited. *Physical Review Fluids*, 2016, **1**, 084502.

[15] Fernandez-Feria R. Note on optimum propulsion of heaving and pitching airfoils from linear potential theory. *Journal of Fluid Mechanics*, 2017, **826**, 781–796.

[16] Heathcote S, Gursul I. Flexible flapping airfoil propulsion at low Reynolds numbers. *AIAA Journal*, 2007, **45**, 1066–1079.

[17] Kang C-K, Aono H, Cesnik C E S, Shyy W. Effects of flexibility on the aerodynamic performance of flapping wings. *Journal of Fluid Mechanics*, 2011, **689**, 32–74.

[18] Quinn D B, Lauder G V, Smits A J. Maximizing the efficiency of a flexible propulsor using experimental optimization. *Journal of Fluid Mechanics*, 2015, **767**, 430–448.

[19] David M J, Govardhan R N, Arakeri J H. Thrust generation from pitching foils with flexible trailing edge flaps. *Journal of Fluid Mechanics*, 2017, **828**, 70–103.

[20] Molina J, Zhang X. Aerodynamics of a heaving airfoil in ground effect. *AIAA Journal*, 2011, **49**, 1168–1179.

[21] Quinn D B, Moored K W, Dewey P A, Smits A J. Unsteady propulsion near a solid boundary. *Journal of Fluid Mechanics*, 2014, **742**, 152–170.

[22] Mivehchi A, Dahl J, Licht S. Heaving and pitching oscillating foil propulsion in ground effect. *Journal of Fluids and Structures*, 2016, **63**, 174–187.

[23] Licht S C, Wibawa M S, Hover F S, Triantafyllou M S. In-line motion causes high thrust and efficiency in flapping foils that use power downstroke. *Journal of Experimental Biology*, 2010, **213**, 63–71.

[24] Esfahani J A, Barati E, Karbasian H R. Fluid structures of flapping airfoil with elliptical motion trajectory. *Computers & Fluids*, 2015, **108**, 142–155.

[25] Yang S C, Liu C, Wu J. Effect of motion trajectory on the aerodynamic performance of a flapping airfoil. *Journal of Fluids and Structures*, 2017, **75**, 213–232.

[26] Smith B L, Glezer A. The formation and evolution of synthetic jets. *Physics of Fluids*, 1998, **10**, 2281–2297.

[27] Cattafesta L N, Sheplak M. Actuators for active flow control. *Annual Review of Fluid Mechanics*, 2011, **43**, 247–272.

[28] Amitay M, Smith D R, Kibens V, Parekh D E, Glezer A. Aerodynamic flow control over an unconventional airfoil using synthetic jet actuators. *AIAA Journal*, 2001, **39**,

361–370.

[29] Kim S H, Kim C. Separation control on NACA23012 using synthetic jet. *Aerospace Science and Technology*, 2009, **13**, 172–182.

[30] Monir H E, Tadjfar M, Bakhtian A. Tangential synthetic jets for separation control. *Journal of Fluids and Structures*, 2014, **45**, 50–65.

[31] Zong H H, van Pelt T, Kotsonis M. Airfoil flow separation control with plasma synthetic jets at moderate Reynolds number. *Experiments in Fluids*, 2018, **59**, 169.

[32] Rehman A, Kontis K. Synthetic jet control effectiveness on stationary and pitching airfoils. *Journal of Aircraft*, 2006, **43**, 1782–1789.

[33] Yen J, Ahmed N A. Parametric study of dynamic stall flow field with synthetic jet actuation. *Journal of Fluids Engineering*, 2012, **134**, 071106.

[34] Taylor K, Amitay M. Dynamic stall process on a finite span model and its control via synthetic jet actuators. *Physics of Fluids*, 2015, **27**, 077104.

[35] Tadjfar M, Asgari E. The role of frequency and phase difference between the flow and the actuation signal of a tangential synthetic jet on dynamic stall flow control. *Journal of Fluids Engineering*, 2018, **140**, 111203.

[36] Wang C L, Tang H. Enhancement of aerodynamic performance of a heaving airfoil using synthetic-jet based active flow control. *Bioinspiration & Biomimetics*, 2018, **13**, 046005.

[37] Wu J, Shu C. Implicit velocity correction-based immersed boundary-lattice Boltzmann method and its applications. *Journal of Computational Physics*, 2009, **228**, 1963–1979.

[38] Lin X J, Guo S H, Wu J, Nan J W. Aerodynamic performance of a flapping foil with asymmetric heaving motion near a wall. *Journal of Bionic Engineering*, 2018, **15**, 636–646.

[39] Lin X J, Wu J, Zhang T W. Performance investigation of a self-propelled foil with combined oscillating motion in stationary fluid. *Ocean Engineering*, 2019, **175**, 33–49.